Stanford Exploration Project, Report 124, April 4, 2006, pages 1–??

Prestack exploding-reflectors modeling for migration velocity analysis

Biondo Biondi

ABSTRACT

I introduce a prestack generalization of exploding-reflectors modeling that has the potential to drastically reduce the computational cost of Migration Velocity Analysis (MVA) based on wavefield-continuation migration and modeling. The method aims at synthesizing, starting form a prestack migrated image, a limited number of independent experiments that contain all the velocity information needed for MVA.
The basic element of the method is the modeling of one isolated Subsurface-Offset Domain Common Image Gather (SODCIG) by using the prestack image as an initial condition. Taking advantage of the limited range of the subsurface offsets in the migrated image, we can combine many SODCIGs in the same modeling experiment without diminishing the velocity information contained in the data. The number of independent experiments required depends on how close we are to the correct migration velocity. Theoretically, this number is the same as the number of subsurface offsets needed to represent the prestack image from which we started the modeling. Several numerical examples illustrate the basic concepts of the proposed method, and demonstrate its potential usefulness for MVA.

INTRODUCTION

We would like to estimate migration-velocity models based on iterative wavefield-continuation migrations, in contrast with the conventional use of iterative Kirchhoff migrations, to take full advantage of the superior imaging capabilities of wavefield-continuation migration. If computational cost were not a consideration, we also should be updating the velocity field using a wavefield tomographic operator (Symes and Carazzone, 1991; Pratt, 1999; Sava and Biondi, 2004a,b) instead of the computationally cheaper conventional ray tomography. Unfortunately, the high computational cost of wavefield migration (and modeling) stands on the way to the practical achievements of these goals.

In this paper I present a method that has the potential of substantially reducing the computational cost of Migration Velocity Analysis (MVA) based on wavefield migration. The method could be applied to both MVA based on conventional ray tomography as well as MVA based on wavefield operators. The computational saving is achieved by synthesizing a new data set that has a number of *independent experiments* lower than the number of shot gathers in the original data set, but that contains all the information needed to estimate migration

velocity. This new data set is synthesized from a prestack image obtained using a wavefield-continuation migration. This initial prestack image is assumed to be only partially focused, with the defocusing related to an inaccurate migration velocity. In principle, the better focused the initial image is, the fewer independent experiments are needed for the new data set to contain all the information needed by MVA.

I propose to synthesize the new data set by applying a prestack generalization of exploding-reflectors modeling. Conceptually, the starting point is the modeling of an isolated Subsurface-Offset Domain Common Image Gathers (SODCIGs). The image in the SODCIGs is used to generate both the source and receiver wavefields at zero time (exploding reflectors). The wavefields are then propagated toward the surface and recorded there by aerial arrays covering the whole surface of the model. The receiver wavefield is propagated forward in time, whereas the source wavefield is propagated backward in time. Any numerical scheme can be used for wave propagation. In particular, both the one-way wave equation and the two-way wave equations can be used for this purpose. The numerical examples I show in this paper are obtained by solving the two-way wave equation in the time domain, because the visual inspection of propagating wavefields provides an intuitive understanding of the process.

Generating an independent experiment for every SODCIG in the prestack image would actually create a data set even larger than the original data set. However, the fundamental observation is that we can simultaneously model several SODCIGs without hampering the velocity analysis based on this reduced data set, as long as we are careful to combine SODCIGs that are sufficiently *uncorrelated*. If the SODCIGs have been focused by migration, albeit imperfectly because of velocity errors, decorrelation can be achieved by taking advantage of the limited range along the subsurface offset axis of the partially focused image.

When the SODCIGs are uncorrelated, the modeling for many SODCIGs can be combined. The data resulting from modeling the combined SODCIGs can be imaged without the contributions of the individual SODCIGs correlating with each other and diminishing the velocity information contained in the migrated image. In this paper I take a simple approach to assure decorrelation; I model SODCIGs defined on several coarse grids which are shifted with respect to each other. In other words, I obtain the initial condition for modeling each independent experiment by multiplying the prestack image by a spatial comb function. I then shift the comb function until the image space is entirely covered. I show that if the distance between adjacent SODCIGs is equal, or larger, than the effective range of offsets in the SODCIGs, the velocity information is preserved. This process reduces to the conventional zero-offset exploding reflectors modeling in the limit that we model all SODCIGs together and assume that they are different from zero only at zero offset. From this viewpoint, the implicit assumption underlying zero-offset exploding-reflectors modeling is that the image is perfectly focused and all the energy is concentrated at zero subsurface offset.

The proposed method can be theoretically analyzed by using concepts that are similar to the ones used to analyze the "cross-talks" in phase-encoding (Romero et al., 2000) and Montecarlo (Cazzola et al., 2004) migration. This theoretical insight suggests that even further saving might be achieved by using temporally uncorrelated and spatially varying source functions. This direction is promising and deserves further work, but is beyond the scope of this

paper.

PRESTACK EXPLODING REFLECTOR MODELING

In this section I discuss the basic concept for modeling SODCIGs and show how the data created by this process contain useful velocity information.

Modeling of an isolated SODCIG

The modeling process starts from the prestack image $I\left(z_\xi, x_\xi, h_\xi\right)$ that is function of the image-space coordinates: depth z_ξ, horizontal location x_ξ, and horizontal subsurface offset h_ξ. We then extract from the whole image a single SODCIG identified by its horizontal coordinate x^i_ξ, and model the corresponding aerial-shot data $D^s_{x^i_\xi}$ and aerial-receiver data $D^g_{x^i_\xi}$ by propagating the source wavefield $P^s_{x^i_\xi}$ and the receiver wavefield $P^g_{x^i_\xi}$ starting from the following initial conditions:

$$P^s_{x^i_\xi}\left(t=0, x=x_\xi - h_\xi, z=z_\xi\right) = I\left(z_\xi, x^i_\xi, h_\xi\right), \tag{1}$$

$$P^g_{x^i_\xi}\left(t=0, x=x_\xi + h_\xi, z=z_\xi\right) = I\left(z_\xi, x^i_\xi, h_\xi\right). \tag{2}$$

The receiver wavefield is propagated forward in time (t), whereas the source wavefield is propagated backward in time.

The modeled-data gathers are generated by extracting the wavefields values at the surface for all times and all surface locations as follows:

$$D^s_{x^i_\xi}(t,x) = P^s_{x^i_\xi}(t,x,z=0), \tag{3}$$

$$D^g_{x^i_\xi}(t,x) = P^g_{x^i_\xi}(t,x,z=0). \tag{4}$$

The simple modeling procedure illustrated above generates data useful for analyzing only flat reflectors. A generalization of this procedure to reflectors with arbitrary dips can be simply achieved by tilting the source function and aligning it along the normal to the reflector instead of along the vertical; that is, by interpreting the offset as the geological-dip offset instead of as the horizontal offset. Biondi and Symes (2004) provide a kinematic analysis of SODCIGs from dipping reflectors that justify the following generalization of equations 1 and 2:

$$P^s_{\alpha x^i_\xi}\left(t=0, x=x_\xi - h_\xi\cos\alpha, z=z_\xi - h_\xi\sin\alpha\right) = I\left(z_\xi, x^i_\xi, h_\xi\right), \tag{5}$$

$$P^g_{\alpha x^i_\xi}\left(t=0, x=x_\xi + h_\xi\cos\alpha, z=z_\xi + h_\xi\sin\alpha\right) = I\left(z_\xi, x^i_\xi, h_\xi\right), \tag{6}$$

and correspondingly,

$$D^s_{\alpha x^i_\xi}(t,x) = P^s_{\alpha x^i_\xi}(t,x,z=0), \tag{7}$$

$$D^g_{\alpha x^i_\xi}(t,x) = P^g_{\alpha x^i_\xi}(t,x,z=0). \tag{8}$$

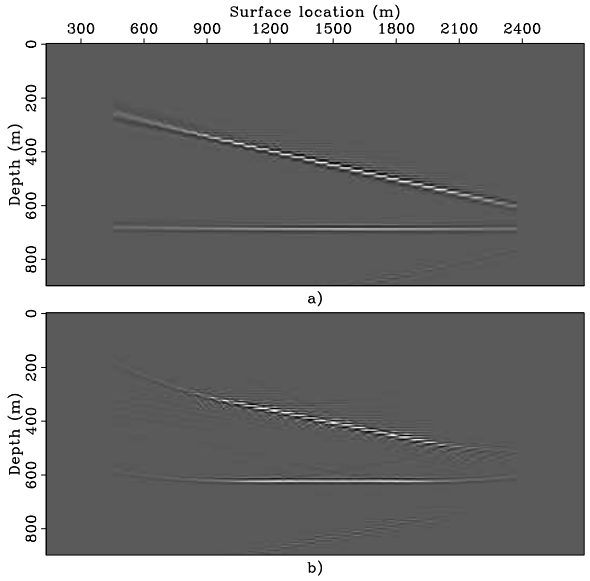

Figure 1: Zero-subsurface-offset sections obtained by source-receiver migration: a) with the correct velocity, and b) a velocity too slow by 10%. biondo1-Sections-overn [ER]

To illustrate the proposed modeling procedure I applied it to a SODCIG extracted from the prestack image of a simple synthetic data set. The data were modeled by using the two-way wave equation and by assuming a constant propagation velocity of 1 km/s and two reflectors: a flat reflector below a reflector dipping by 10 degrees. The complete data set comprises a total of 100 split-spread shot gathers. I migrated the data twice by source-receiver migration: once using the correct velocity and once using a velocity too slow by 10%. Figure 1, shows the zero-subsurface-offset sections obtained by migration with the correct velocity (Figure 1a), and a velocity too slow by 10% (Figure 1b). Figure 2 shows snapshots of the wavefields obtained by extracting an individual SODCIG from the prestack image obtained using the correct velocity (Figure 1a). Panel a) shows the source wavefield and panel b) shows the receiver wavefield. Figure 3 shows the data recorded at the surface by the aerial arrays corresponding to the wavefields shown in Figure 2. Notice that the source wavefield (panel a) is recorded at negative times, because it is propagated back in time. Figures 4–5 shows wavefields snapshots and the recorded data corresponding to the same SODCIG used to model the data shown in Figure 3, but assuming the reflectors to be dipping by 45 degrees, and imposing the initial conditions expressed in equations 5 and 6. Notice that, because of the assumed reflector dip, the wavefields shown in Figure 4 are more asymmetric than the the wavefields shown in Figure 2, with the receiver wavefield (Figure 2b) tilted towards the right more than the source wavefield (Figure 2a).

Migration

The experiment modeled following the procedure described above can be imaged by using conventional migration of aerial shot data. For example, the reverse time migration of the data can be expressed as:

$$\overline{I_i}\left(z_\xi, x_\xi, h_\xi\right) = \sum_t \overline{P^s}_{\alpha x^i_\xi}\left(t, z=z_\xi, x=x_\xi - h_\xi\right) \overline{P^g}_{\alpha x^i_\xi}\left(t, z=z_\xi, x=x_\xi + h_\xi\right), \qquad (9)$$

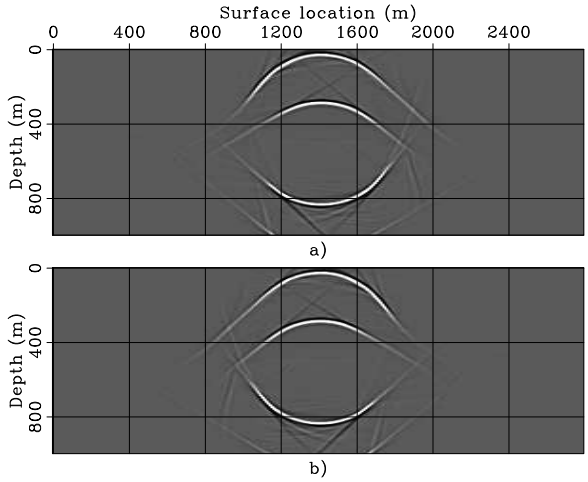

Figure 2: Snapshots of the source wavefield (panel a) and the receiver wavefield (panel b) generated by modeling an isolated SOD-CIG by imposing the initial conditions expressed in equations 1 and 2. biondo1-Snaps-INF-overn [ER]

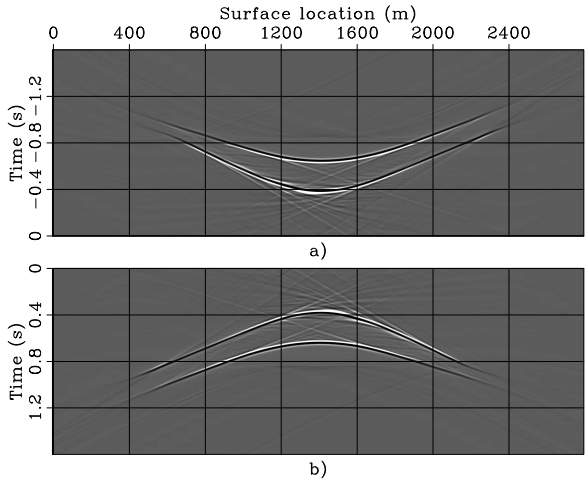

Figure 3: The data recorded at the surface by aerial arrays and corresponding to the source wavefield (panel a) and the receiver wavefield (panel b) shown in Figure 2. biondo1-Data-INF-overn [ER]

where the source and receiver data provide the surface boundary conditions to generate the source wavefield $\overline{P}^s{}_{\alpha x^i_\xi}$ and the receiver wavefield $\overline{P}^g{}_{\alpha x^i_\xi}$.

To theoretically analyze the migration results we can express these wavefields as function of the data convolved, both in time and space, with the convolutional operator G_1, that represents the propagation from the surface into the subsurface. For the sake of simplicity, I limit this analysis to the flat-reflector case, where the wavefields at depth can be written as:

$$\overline{P}^s{}_{x^i_\xi}(t,x,z) = G_1(x,z=0;x,z) * D^s_{x^i_\xi}(t,x), \tag{10}$$

$$\overline{P}^g{}_{x^i_\xi}(t,x,z) = G_1(x,z=0;x,z) * D^g_{x^i_\xi}(t,x). \tag{11}$$

Similarly, the data themselves can be represented as the convolution of the image (exploding reflectors) with the operator G_0 representing the propagation from the subsurface up to the surface; that is, as:

$$D^s_{x^i_\xi}(t,x) = G_0\left(x = x^i_\xi - h_\xi, z = z_\xi; x, z = 0\right) * I\left(z_\xi, x^i_\xi, h_\xi\right), \tag{12}$$

$$D^g_{x^i_\xi}(t,x) = G_0\left(x = x^i_\xi + h_\xi, z = z_\xi; x, z = 0\right) * I\left(z_\xi, x^i_\xi, h_\xi\right). \tag{13}$$

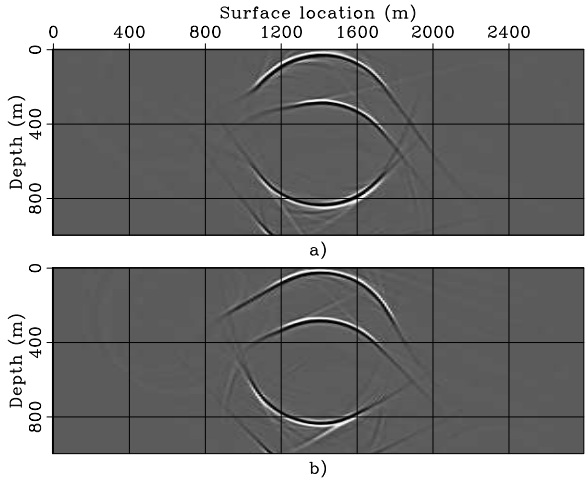

Figure 4: Snapshots of the source wavefield (panel a) and the receiver wavefield (panel b) generated by modeling an isolated SODCIG by imposing the initial conditions expressed in equations 5 and 6 and assuming a reflector dip of 45 degrees. biondo1-Snaps-INF-DIP-overn [ER]

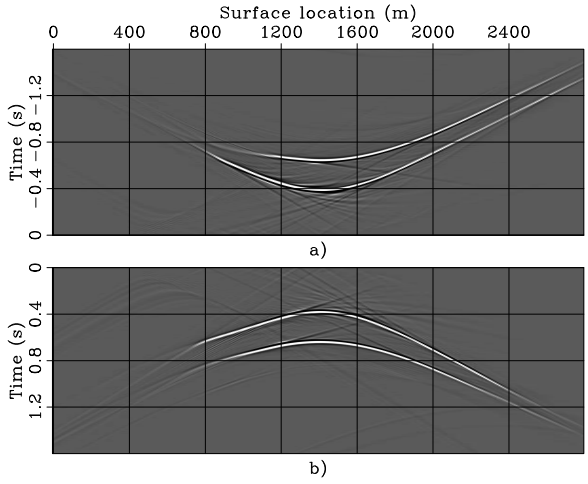

Figure 5: The data recorded at the surface by aerial arrays and corresponding to the source wavefield (panel a) and the receiver wavefield (panel b) shown in Figure 4. biondo1-Data-INF-DIP-overn [ER]

Substituting equation 12 into equation 10, and equation 13 into equation 11, I obtain:

$$\overline{P^s}_{x_\xi^i}(t,x,z) = G_1(x,z=0;x,z) * G_0\left(x=x_\xi^i-h_\xi,z=z_\xi;x,z=0\right) * I\left(z_\xi,x_\xi^i,h_\xi\right), \quad (14)$$

$$\overline{P^g}_{x_\xi^i}(t,x,z) = G_1(x,z=0;x,z) * G_0\left(x=x_\xi^i+h_\xi,z=z_\xi;x,z=0\right) * I\left(z_\xi,x_\xi^i,h_\xi\right), \quad (15)$$

In general, the velocity models used for modeling and migration may be different, and thus the forward and backward propagators G_0 and G_1 are not the "inverse" of each other. Their convolution can be expressed as:

$$\Delta G(x_0,z_0;x_1,z_1) = G_0(x=x_0,z_0;x,z=0) * G_1(x,z=0;x=x_1,z_1). \quad (16)$$

When the modeling and migration velocity functions are the same, the convolutional operator ΔG is concentrated around $(x_0=x_1,z_0=z_1)$; otherwise, it shifts the wavefields proportionally to the differences between the velocities.

Substituting equation 14 and 15 into equation 9, I obtain the following expression for the

image after migration

$$\begin{aligned}\overline{I_i}\left(z_\xi, x_\xi, h_\xi\right) \\ = \sum_t \quad & G_1\left(x, z=0; x = x_\xi - h_\xi, z = z_\xi\right) * G_0\left(x = x_\xi^i - h'_\xi, z = z'_\xi; x, z=0\right) * I\left(z'_\xi, x_\xi^i, h'_\xi\right) \\ & G_1\left(x, z=0; x = x_\xi + h_\xi, z = z_\xi\right) * G_0\left(x = x_\xi^i + h'_\xi, z = z'_\xi; x, z=0\right) * I\left(z'_\xi, x_\xi^i, h'_\xi\right),\end{aligned} \tag{17}$$

and then substituting equation 16 into equation 17 we get:

$$\begin{aligned}\overline{I_i}\left(z_\xi, x_\xi, h_\xi\right) \\ = \sum_t \quad & \left[\Delta G\left(x_\xi^i - h_\xi, z_\xi; x_\xi^i - h'_\xi, z'_\xi;\right) * I\left(z'_\xi, x_\xi^i, h'_\xi\right)\right] \\ & \left[\Delta G\left(x_\xi^i + h_\xi, z_\xi; x_\xi^i + h'_\xi, z'_\xi;\right) * I\left(z'_\xi, x_\xi^i, h'_\xi\right)\right].\end{aligned} \tag{18}$$

When the velocities are the same the migrated image $\overline{I_i}$ is an approximation of the square of the starting image I. When the migration velocity is different from the modeling velocity, the two images may substantially differ. Because we want to use migration results to estimate velocity, it is important to demonstrate that the velocity information contained in the prestack image obtained from the data modeled using the proposed procedure is consistent with the velocity information extracted from the prestack image obtained from migrating the whole data set.

Figure 6 shows the SODCIGs and the Angle Domain Common Image Gathers (ADCIGs) obtained by migrating the data sets shown in Figures 3 and 5, and compares these ADCIGs with the ADCIG (Figure 6e) computed from the SODCIG used as initial condition for modeling. The ADCIGs show the same kinematics (all three of them are flat), though the amplitudes in the ADCIGs obtained by migrating the data modeled by the proposed method is lower at wide aperture angles. This difference is likely to be related to the Jacobian of imaging, similarly to the phenomenon analyzed by Sava et al. (2004) for downward-continuation migration and modeling. It warrants further investigations.

Figure 7 shows the SODCIGs and the ADCIGs obtained by migrating the data sets shown in Figures 3 and 5 with a migration velocity too slow by 10%. The last panel (Figure 7e) shows the ADCIG computed from the prestack image obtained by source-receiver migration of the original 100-shots data set with a migration velocity too slow by 10%. The residual moveouts caused by the velocity error are the same for the ADCIG obtained by migrating the data modeled starting from an isolated SODCIG and by migrating the original data set.

COST-EFFICIENT PRESTACK EXPLODING-REFLECTOR MODELING

The independent modeling and imaging of all SODCIGs in a prestack image would be computationally expensive. However, several SODCIG can be modeled together, thus drastically reducing the number of independent experiment that must be modeled and imaged. The combinations of the several SODCIG can be expressed as the following summation:

$$I_j\left(z_\xi, x_\xi, h_\xi\right) = \sum_{i \in A_j} I\left(z_\xi, x_\xi^i, h_\xi\right), \tag{19}$$

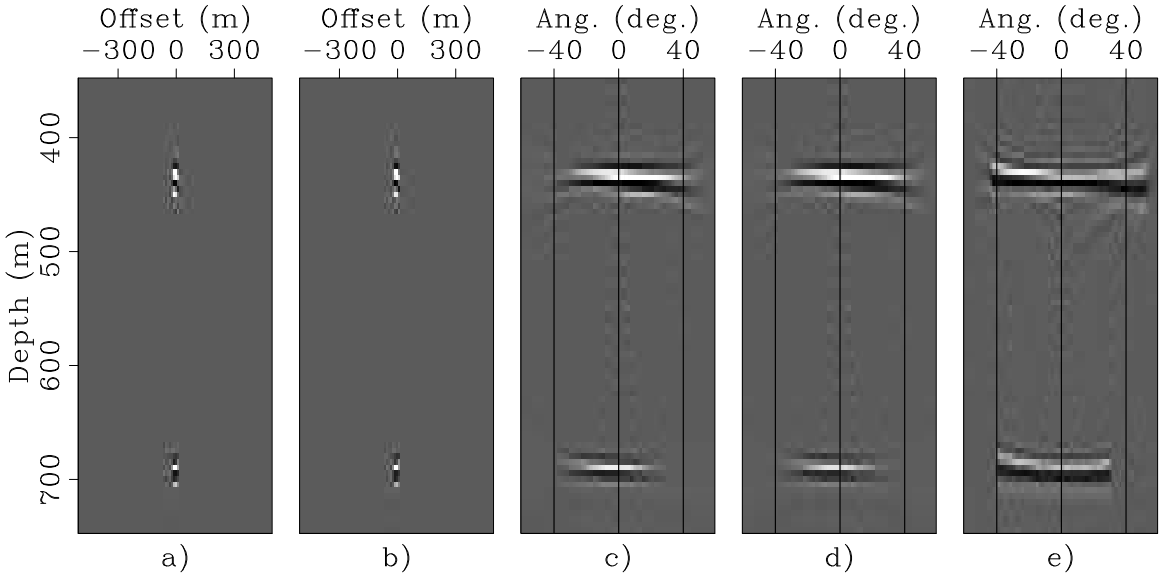

Figure 6: SODCIGs and ADCIGs computed from the data shown in Figures 3 and 5: SODCIG from "flat-reflector" data (panel a), SODCIG from "dipping-reflector" data (panel b), ADCIG from "flat-reflector" data (panel c), ADCIG from "dipping-reflector" data (panel d), ADCIG computed from the SODCIG used as initial condition for modeling (panel e). biondo1-Mig-Angs-INF-overn [ER]

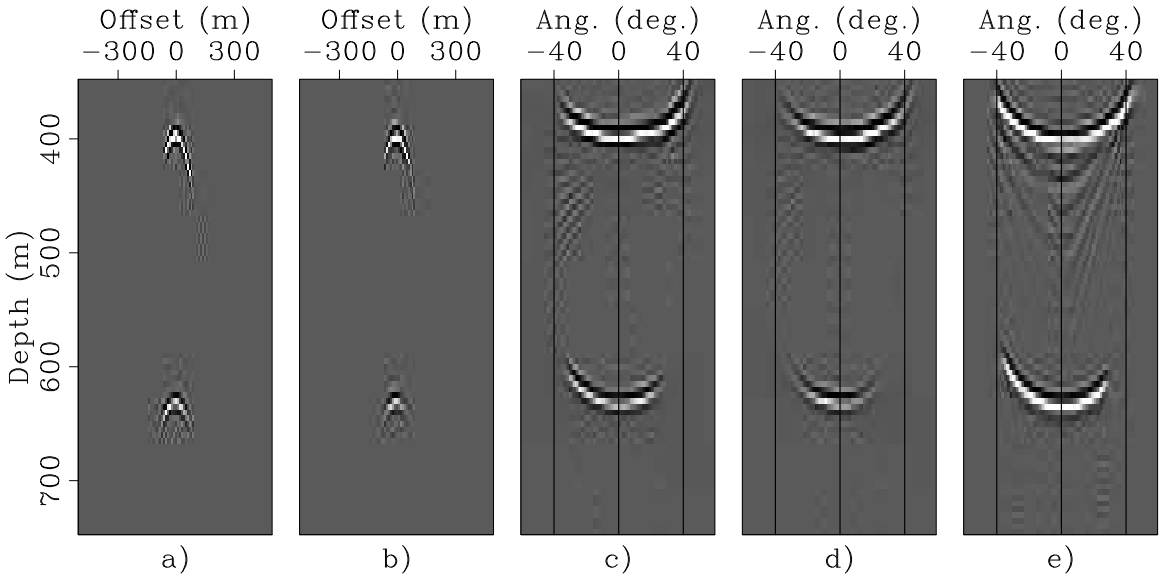

Figure 7: SODCIGs and ADCIGs computed from the data shown in Figures 3 and 5 and migrated with a velocity too slow by 10%: SODCIG from "flat-reflector" data (panel a), SODCIG from "dipping-reflector" data (panel b), ADCIG from "flat-reflector" data (panel c), ADCIG from "dipping-reflector" data (panel d), ADCIG computed by a source-receiver migration of the original 100-shots data set with a velocity too slow by 10% (panel e). biondo1-Mig-Angs-INF-SLOW-overn [ER]

where A_j is the set of SODCIGs combined for creating one single modeling experiment.

Because of the linearity of equations 12 and 13, the data computed by modeling the subset A_j can be expressed as the sum of the data sets obtained by modeling each x_ξ^i independently; that is,

$$\widehat{D_j^s}(t,x) = \sum_{i\in A_j} D^s_{x_\xi^i}(t,x), \tag{20}$$

$$\widehat{D_j^g}(t,x) = \sum_{i\in A_j} D^g_{x_\xi^i}(t,x). \tag{21}$$

The result of migrating this combined data set can be written as follows:

$$\begin{aligned}
&\widehat{I_j}\left(z_\xi,x_\xi,h_\xi\right)\\
&\quad = \textstyle\sum_{i\in A_j} && \left[\Delta G\left(x_\xi^i-h_\xi,z_\xi;x_\xi^i-h'_\xi,z'_\xi;\right)*I\left(z'_\xi,x_\xi^i,h'_\xi\right)\right]\\
&\quad && \left[\Delta G\left(x_\xi^i+h_\xi,z_\xi;x_\xi^i+h'_\xi,z'_\xi;\right)*I\left(z'_\xi,x_\xi^i,h'_\xi\right)\right]\\
&\quad + \textstyle\sum_{k\in A_j;k\neq l}\sum_{l\in A_j} && \left[\Delta G\left(x_\xi^l-h_\xi,z_\xi;x_\xi^l-h'_\xi,z'_\xi;\right)I\left(z'_\xi,x_\xi^l+h'_\xi,h'_\xi\right)\right]\\
&\quad && \left[\Delta G\left(x_\xi^k-h_\xi,z_\xi;x_\xi^k-h'_\xi,z'_\xi;\right)I\left(z'_\xi,x_\xi^k-h'_\xi,h'_\xi\right)\right].
\end{aligned} \tag{22}$$

The first term in equation 22 is the desired result; that is, the image that we would obtain if we had independently modeled and imaged each SODCIG belonging to A_j, and summed the results. The second term in equation 22 represents the "cross-talk" between the SODCIGs; these artifacts are the unwanted consequence of combining SODCIGs before modeling in order to save computations.

The second term in equation 22 becomes easier to analyze in the special case when migration velocity is the same as the modeling velocity. The "residual propagation" operator ΔG thus approximates a delta function and equation 22 simplifies into:

$$\widehat{I_j}\left(z_\xi,x_\xi,h_\xi\right) \approx \sum_{i=1}^{N} I^2\left(z_\xi,x_\xi^i,h_\xi\right) + \sum_{k\in A_j;k\neq l}\sum_{l\in A_j} I\left(z_\xi,x_\xi^i+h_\xi,h_\xi\right)I\left(z_\xi,x_\xi^k-h_\xi,h_\xi\right). \tag{23}$$

In this case, the the cross-talks terms are given by the product of each SODCIG in A_j, shifted by the subsurface offset h_ξ, with all the other SODCIG in A_j, shifted by $-h_\xi$. If we assume that the SODCIGs have limited subsurface offset range because they are partially focused by migration, we can easily eliminate the cross-talks interference with the desired image in a window around zero subsurface offset by ensuring that the SODCIG belonging to A_j are sufficiently separated in space. The numerical examples in the next section demonstrates this point.

However, if the migration and modeling velocities are dissimilar, the shifted versions of the SODCIGs contributing to the cross-talk are distorted and shifted by the "residual propagation" operator ΔG (equation 22). This additional shift may increase, or decrease, the amount of interference of the cross talks with the desired image. The last example in the next section illustrates this point.

Synthetic data examples

To test the analytical results presented in the previous section, I modeled and migrated several data sets that combined SODCIGs extracted from the prestack images of the synthetic data set described above. The SODCIGs were uniformly spaced with four choices for their distance Δx_ξ^i: 640 meters, 320 meters, 160 meters, and 80 meters. The original midpoint spacing of the image, Δx_ξ, was 10 meters. Therefore, the first data set required 64 independent modeling experiments, the second 32, the third 16 and the fourth 8.

Figure 8 compares the SODCIG extracted from the starting prestack image (Figure 8a) with the corresponding SODCIGs extracted from the images obtained by migrating the four combined data sets with the correct velocity. All the SODCIGs have been extracted at the same horizontal location. As predicted by equation 23, the images obtained by the combined data sets are affected by cross talk along the offset domain. The images obtained from the smaller data set that had only 8 independent experiments (Figure 8e) is completely degraded by the cross-talk. Whereas the larger data sets (Δx_ξ^i equal to 320 and 640 meters) preserve the velocity information present in the original SODCIG and allow the computation of ADCIGs uncontaminated by artifacts, after the cross-talks are removed by limiting the offset aperture.

Figure 9 shows the same SODCIGs shown in Figure 8 after the larger subsurface offsets are zeroed. Because the distance between cross-talks decreases with decreasing Δx_ξ^i, the windows around zero offset also decreases in width. For Figure 9b the window was 410 meters wide, for Figure 9c it was 170 meters wide, for Figure 9d it was 110 meters wide, for Figure 9e it was 70 meters wide. Figure 10 shows the ADCIGs obtained by transforming into the angle domain the SODCIGs shown Figure 9. The ADCIGs computed by imaging the larger data sets (Δx_ξ^i equal 320 and 640 meters) preserve the velocity information contained in the original ADCIG (Figure 10a), whereas the ADCIG computed from the data set with only 8 independent experiments (Figure 10e), is completely overwhelmed by artifacts.

The amount of interference caused by the cross-talk also depends on how well the SODCIGs are focused around zero subsurface offset, in addition to the spacing between SODCIGs. When the initial migration is not perfectly focused because of velocity inaccuracies, more experiments are needed to preserve the velocity information than when the starting image is well focused. Figure 11, illustrating this concept, shows the SODCIGs obtained starting from the prestack image computed by source-receiver migration using a migration velocity too low by 10%. Figure 11 shows the original SODCIG, whereas the other panels show the SODCIG obtained with increasingly smaller data sets, as in Figure 8. Because of the velocity error the SODCIGs are not well focused at zero offset. In this case, only the data set with 64 independent experiments produces a SODCIG with the cross-talk sufficiently separated from zero offset not to interfere with the desired image.

This result is confirmed by the transformation to angle domain. Figure 12 shows the ADCIGs obtained after windowing the SODCIGs shown in Figure 11. The ADCIG obtained by migrating all the 64 independent experiments (Figure 12b) contains the same velocity information as the original ADCIG (Figure 12a), whereas the others are affected by artifact caused by the cross talks, increasingly so going from left to right in the figure. The two previ-

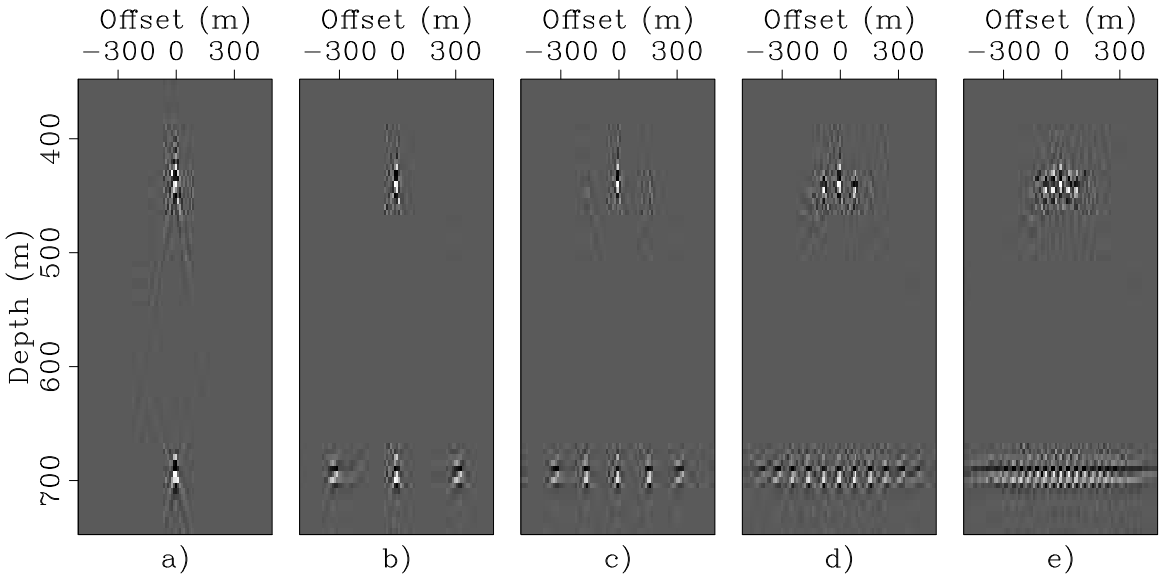

Figure 8: Panel a): SODCIG extracted from source-receiver migration of synthetic data set migrated with correct velocity. Panels b) to e): SODCIGs obtained from migration of data sets modeled using the proposed method, with respectively $\Delta x_\xi^i = 640$ m, 320 m, 160 m and 80 m. biondo1-Migs-nowind-overn [CR]

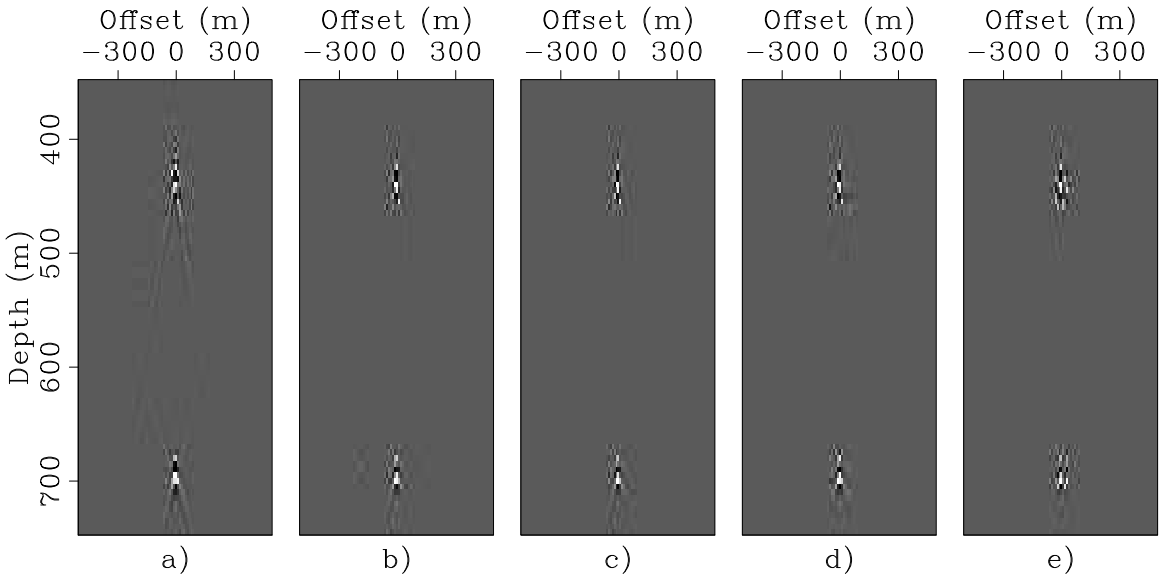

Figure 9: Same panels shown in Figure 8 after zeroing the larger subsurface offsets to maximally eliminate the cross-talk before transformation to angle domain (Figure 10). biondo1-Migs-wind-overn [CR]

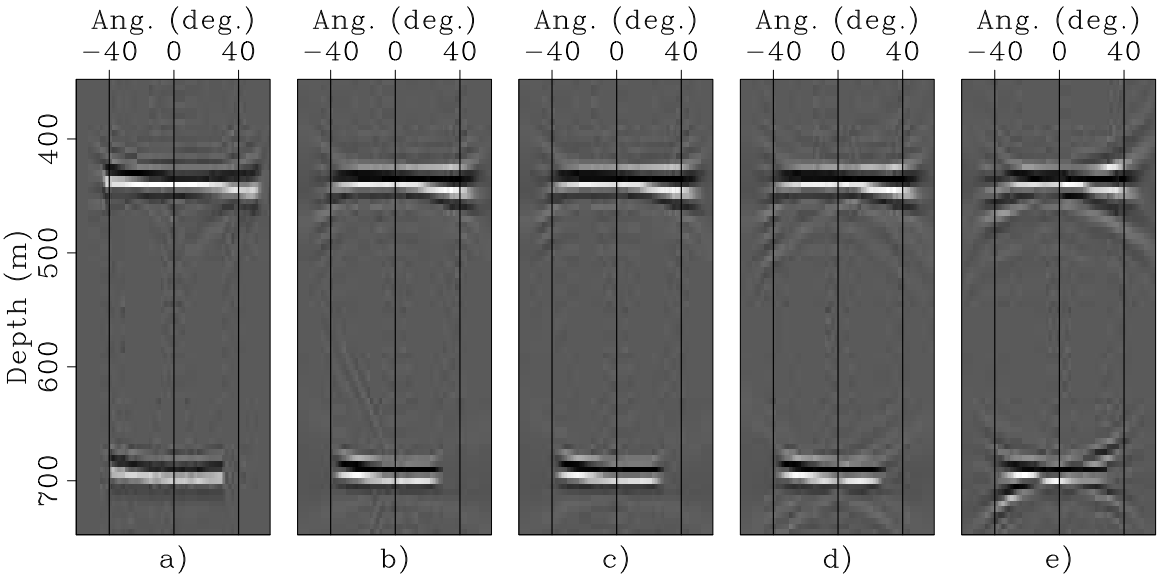

Figure 10: ADCIGs obtained by transformation of the windowed SODCIGs shown in Figure 9. Panel a): ADCIG computed from source-receiver migration of synthetic data set migrated with correct velocity. Panels b) to e): ADCIGs obtained from the migration of data sets modeled using the proposed method, with respectively $\Delta x_\xi^i = 640$ m, 320 m, 160 m and 80 m. biondo1-Angs-wind-overn [CR]

ous examples display the imaging results when the modeling and migration velocity were the same. However, because the proposed modeling method would be used for MVA, which requires iterative migrations with different velocities, it is useful to evaluate the results when the modeling and migration velocities differ. Therefore, I modeled four data sets, again with decreasing Δx_ξ^i; I started as before with Δx_ξ^i= 640 meters, and went down to 320 meters, 160 meters and 80 meters. The starting image was obtained by source-receiver migration with velocity too slow by 10%. The data were modeled assuming the same low velocity, but they were migrated using the correct velocity, and thus the SODCIGs after migration are now well focused.

Figure 13 shows the resulting SODCIGs and compares them with the well-focused SODCIGs obtained by source-receiver migration of the original data set with the correct velocity (Figure 13a). As in Figure 8, the cross-talk artifacts in the SODCIGs obtained by migrating the data sets formed by 32 and 64 independent experiments are sufficiently far from zero offset to be easily zeroed before transformation to angle domain. Figure 14 shows the corresponding ADCIGs, which show flat moveout for the deep flat reflector. A small residual moveout can be observed for the shallow dipping reflector that is probably related to staircase artifacts in the initial modeling. In other words, because of the coarseness of the modeling grid, the dipping reflector behaves as a sequence of short segments of flat reflectors, instead as a continuous planar reflector dipping at 10 degrees. All ADCIGs, except the ones shown in Figure 14d and 14e are free from artifacts and provide useful velocity information.

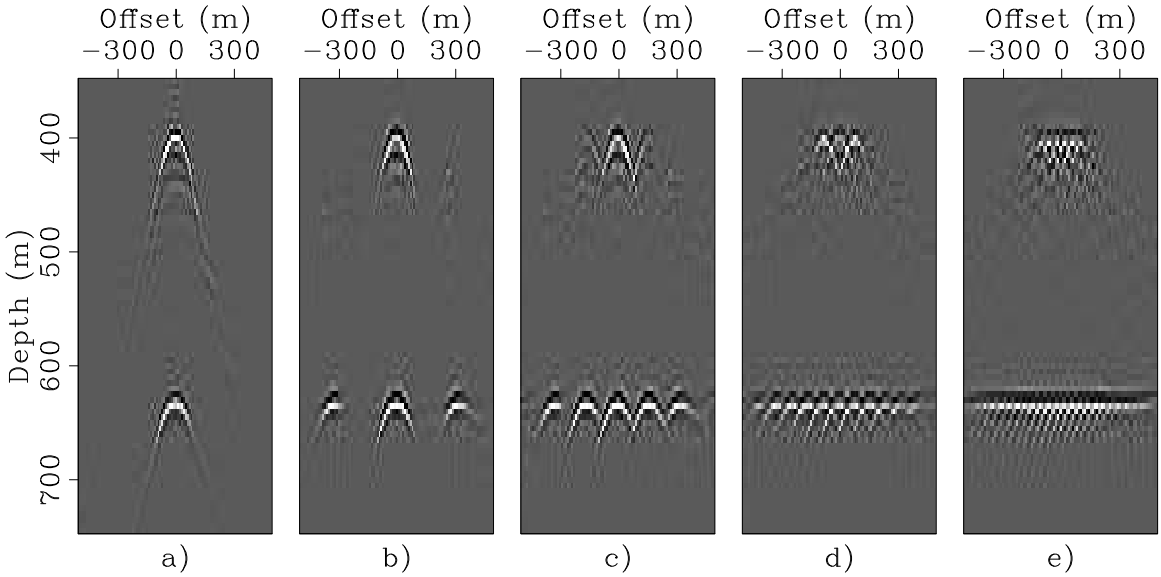

Figure 11: Panel a): SODCIG extracted from source-receiver migration of synthetic data set migrated with velocity too slow by 10%. Panels b) to e): SODCIGs obtained from migration of data sets modeled using the proposed method, with respectively $\Delta x_\xi^i = 640$ m, 320 m, 160 m and 80 m. The modeling and the migration velocities were the same and both too slow by 10%. biondo1-Migs-slow-nowind-overn [CR]

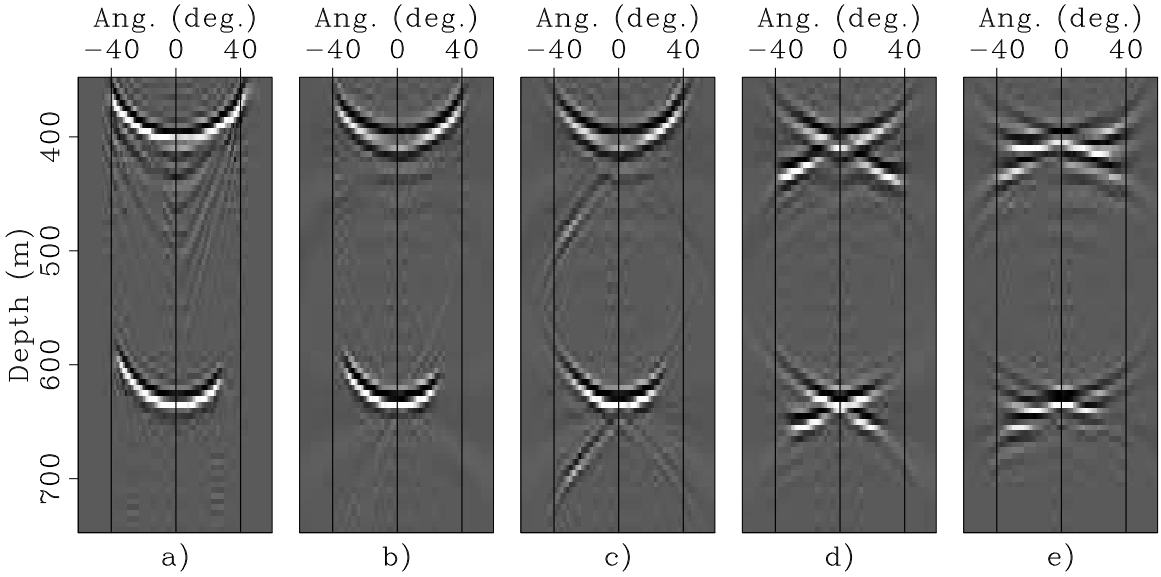

Figure 12: ADCIGs obtained by transformation of the SODCIGs shown in Figure 11 after windowing. Panel a): ADCIG computed from source-receiver migration of synthetic data set migrated with velocity too slow by 10%. Panels b) to e): ADCIGs obtained from migration of data sets modeled using the proposed method, with respectively $\Delta x_\xi^i = 640$ m, 320 m, 160 m and 80 m. biondo1-Angs-slow-wind-overn [CR]

The last example illustrates the idea that the interference between SODCIGs depends on the amount of focusing of the SODCIG after migration, not in the starting image. In other words, the "residual propagation" operator ΔG present in equation 22 may decrease, or increase, the amount of cross-talk artifacts, depending whether it improves, or degrades, the focusing of the image.

CONCLUSIONS AND FUTURE DIRECTIONS

The proposed prestack exploding-reflectors modeling preserves the velocity information in the starting prestack image. Taking advantage of the limited subsurface-offset range of partially focused images, several SODCIGs can be combined without degrading the velocity information necessary for MVA. My first tests of the method demonstrate that the number of independent experiments required for MVA can be substantially lower than the number of shot profiles in the original data set. They indicate that minimum number of independent experiments depends on the degree of focusing of the migrated image. The proposed method has the potential of significantly reducing the computational cost of MVA based on wavefield continuation migration and modeling, and to enable the use of expensive wavefields methods when estimating migration velocity.

The number of SODCIG that can be combined to form an independent experiment depends on the degree of correlation between the SODCIGs. In this paper I presented a simple schemes for combining SODCIGs that takes advantage of their limited offset range to achieve spatial decorrelation. However, temporal decorrelation can be also induced by modeling using spatially varying, and temporally decorrelated, source functions. This approach would follow the ideas used for phase encoding and Montecarlo migration. The additional degrees of freedom introduced by the variations in source functions are likely to enable further reduction of the number of independent experiments needed to preserve the velocity information necessary to improve velocity by MVA.

REFERENCES

Biondi, B. and W. W. Symes, 2004, Angle-domain common-image gathers for migration velocity analysis by wavefield-continuation imaging: Geophysics, **69**, 1283–1298.

Cazzola, L., L. Pizzaferri, et al., 2004, An example of wavefield depth migration and Monte Carlo imaging in West Africa deep waters: 74th Ann. Internat. Mtg., Soc. of Expl. Geophys., Expanded Abstracts, 1037–1040.

Pratt, R. G., 1999, Seismic waveform inversion in the frequency domain, Part 1: Theory and verification in a physical scale model: Geophysics, **64**, 888–901.

Romero, L. A., D. C. Ghiglia, C. C. Ober, and S. A. Morton, 2000, Phase encoding of shot records in prestack migration: Geophysics, **65**, 426–436.

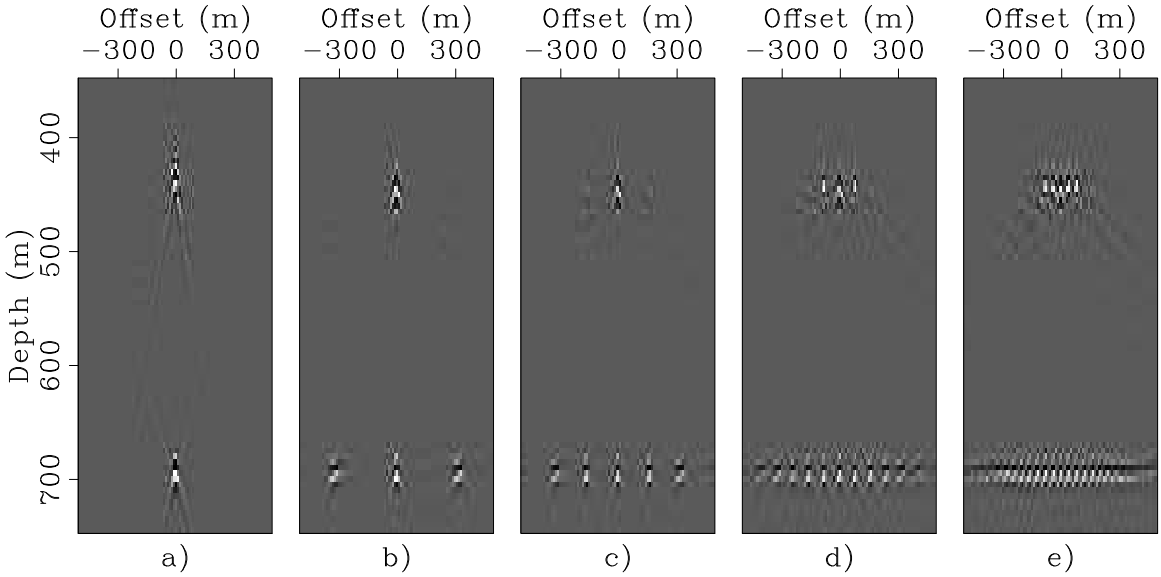

Figure 13: Panel a): SODCIG extracted from source-receiver migration of synthetic data set migrated with velocity too slow by 10%. Panels b) to e): SODCIGs obtained from migration of data sets modeled using the proposed method, with respectively $\Delta x_\xi^i = 640$ m, 320 m, 160 m and 80 m. The modeling velocity was too slow by 10%, but the migration velocity equaled the correct velocity. biondo1-Migs-slow-slow-nowind-overn [CR]

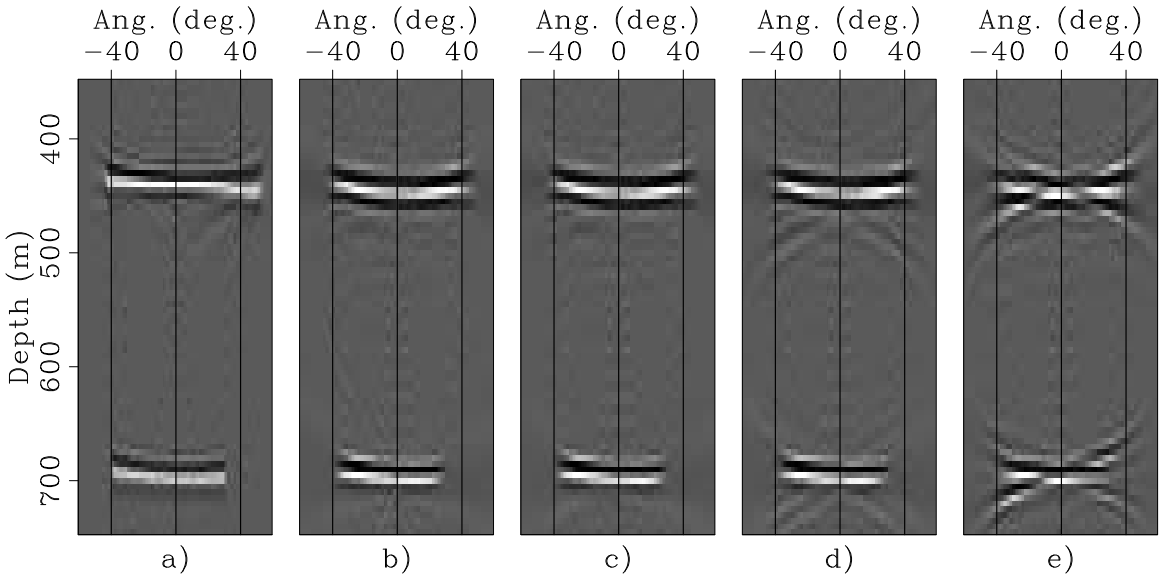

Figure 14: ADCIGs obtained by transformation of the SODCIGs shown in Figure 13 after windowing. Panel a): ADCIG computed from source-receiver migration of synthetic data set migrated with velocity too slow by 10%. Panels b) to e): ADCIGs obtained from migration of data sets modeled using the proposed method, with respectively $\Delta x_\xi^i = 640$ m, 320 m, 160 m and 80 m. The modeling velocity was too slow by 10%, but the migration velocity equaled the correct velocity. biondo1-Angs-slow-slow-wind-overn [CR]

Sava, P. and B. Biondi, 2004a, Wave-equation migration velocity analysis—I: Theory: Geophysical Prospecting, **52**, 593–623.

Sava, P. and B. Biondi, 2004b, Wave-equation migration velocity analysis—II: Examples: Geophysical Prospecting, **52**, 607–623.

Sava, P., B. Biondi, and S. Fomel, 2004, Amplitude-preserved common image gathers by wave-equation migration: 71st Ann. Internat. Mtg., Soc. of Expl. Geophys., Expanded Abstracts, 296–299.

Symes, W. W. and J. J. Carazzone, 1991, Velocity inversion by differential semblance optimization: Geophysics, **56**, 654–663.